ELSEVIER

Journal of Power Sources 112 (2002) 13–29

JOURNAL OF POWER SOURCES

www.elsevier.com/locate/jpowsour

Kinetics of methanol-steam reformation in an internal reforming fuel cell

S.R. Samms*, R.F. Savinell

Department of Chemical Engineering, E.B. Yeager Center for Electrochemical Sciences, Case Western Reserve University, Cleveland, OH 44106, USA

Accepted 16 February 2002

Abstract

A study of the kinetics of the methanol-steam reformation reaction within an idealized tube reactor and within a non-ideal internal reforming fuel cell (IRFC) was performed. Kinetic expressions were calculated from the reaction rate data obtained from the tube reactor by least squares fitting to general power law model, as well as to a mechanism-based model put forth by Peppley et al. [Appl. Catal. A 179 (1999) 21; Appl. Catal. A 179 (1999) 31] assuming isothermal plug flow behavior. Reaction rate data obtained from an IRFC with and without an H_3PO_4 containing membrane electrode assembly (MEA) was compared to the reaction rates predicted by the kinetic model. It was found that methanol conversion rates in the IRFC were significantly less than would be for an ideal plug flow reactor (PFR) with an equal amount of catalyst due to the non-ideal flow through the reactor bed. However, despite the non-ideal flow caused by the design compromises inherent in an IRFC and the resulting drop in effective catalyst activity, it was projected that for fuel cell systems with a current density greater than 400 mA cm^{-2}, the IRFC would require less catalyst mass than a traditional system with external reformer. This is the result of an experimentally verified accelerated methanol conversion rate in the IRFC caused by the extraction of H_2 from the reforming reactor bed. Long-term stability of the IRFC due to acid leaching still needs to be addressed. Additionally, the extraction of H_2 from the reformer bed, which occurs in the IRFC, introduces concerns of failure due to coking.

Keywords: Methanol; In situ; Reforming; Reformation; Kinetics; Fuel cell

1. Introduction

1.1. Motivation

The last decade has witnessed a sudden increase in fuel cell related research and development. The predominance of this research has been focused on automotive applications due to its enormous potential market size. The leader in this technological race has been the hydrogen-fed low-temperature PEM type fuel cell, the most common of which is the Nafion®-based cell. Unfortunately, commercial development of mobile systems based on low-temperature fuel cells has been severely hampered by difficulties associated with transporting and storing of the hydrogen fuel.

Because of methanol's high energy density and the ease with which it can be converted to hydrogen, onboard reforming of methanol is a proposed solution, but one which has been complicated by the low-temperature PEM fuel cell's intolerance of carbon monoxide. Despite significant research effort in this area, low-temperature PEM fuel cells commonly require carbon monoxide levels to be less than 100 ppm, or even as low as 20 ppm for acceptable performance [1]. Typically, the methanol-steam reformation process produces between one and two percent carbon monoxide (depending on reactor temperature and on feed composition) along with the desired products of carbon dioxide and hydrogen. In order to reduce the concentration of carbon monoxide to levels that can be tolerated by the low-temperature fuel cell, fuel-processing systems usually incorporate a water-gas shift reactor as well as a preferential-oxidation reactor to purify the gas produced by the reforming reactor [2].

In response to the challenges facing the development of mobile hydrogen-fed low-temperature PEM fuel cell, researchers at the E.B. Yeager Center for Electrochemical Sciences have developed a PEM fuel cell that is able to operate at temperatures up to ca. 250 °C by using polybenzimidazole (PBI) film equilibrated with phosphoric acid

* Corresponding author. Present address: Motorola Energy Technologies Labs, 7700 South River Parkway, MD ML 28, Tempe, AZ 85284, USA. Tel.: +1-480-755-5650.
E-mail address: stephen.samms@motorola.com (S.R. Samms).

0378-7753/02/$ – see front matter
PII: S0378-7753(02)00089-7

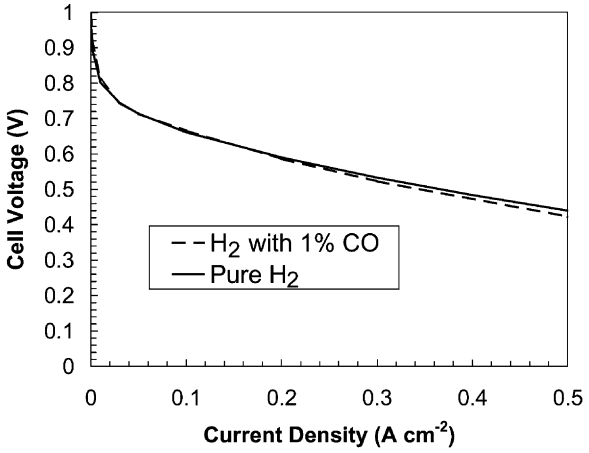

Fig. 1. PBI fuel cell performance with neat hydrogen as compared with 1% CO in hydrogen. Cathode loading of 2.6 mg cm^{-2}, operating on O_2 humidified at room temperature. The temperature of the fuel cell was 170 °C.

as an electrolyte [3]. The primary advantage of operating at higher temperature is that above ca. 150 °C the standard carbon-supported high surface area platinum electrodes become tolerant to relatively high concentrations of carbon monoxide. Experimental data demonstrating the tolerance of a PBI fuel cell operating at 170 °C to carbon monoxide is shown in Fig. 1. The obvious advantage of this type of fuel cell is that it is no longer necessary for the fuel-processing system to remove the bulk of carbon monoxide from the reformate gas, effectively eliminating the need for a water-gas shift reactor and a preferential-oxidation reactor. A less obvious advantage of a PBI-based fuel cell is that the fuel cell can now be operated at a temperature exceeding the temperature required to steam-reform methanol. With this arrangement, the excess heat produced by the operation of the fuel cell can now be used to drive the endothermic reforming reaction, whereas the heat produced by the operation of a low-temperature PEM fuel cell is usually at too low of a temperature to be of much use.

The advantages of the PBI-based fuel cell are utilized in the design of the internal reforming fuel cell (IRFC). Carbon monoxide tolerance allows the fuel processor to be designed as a single (reforming) stage and the higher temperature of operation allows the single stage fuel processor to be integrated into the fuel cell itself. To accomplish the integration, commercial low-temperature methanol-steam reformation catalyst, BASF K3-110, was placed in the gas flow channels of the fuel cell's anodic current collecting plate, as shown in Fig. 2. The IRFC was then operated at a temperature of 225 °C and fed a mixture of methanol and water to the anode. As the feed mixture enters the anodic chamber of the fuel cell, the methanol is catalytically steam reformed to form a mixture of H_2, CO_2, and CO. The hydrogen diffuses to the anode, located directly adjacent to the catalyst bed, where it is electrochemically oxidized, generating electricity and heat, the latter is used to drive the endothermic reforming reaction.

1.2. Theoretical advantages of the internal reforming fuel cell

There are four primary theoretical advantages of integrating the reformer into the fuel cell: (1) simplification of the design; (2) increased overall efficiency; (3) minimization of system weight and volume; and (4) inherent dynamic stability. The reasons behind each of these advantages are briefly explained below, but before doing so, it should be noted that the objective of this work is not to prove or disprove all of the theoretical advantages. That would entail a much more extensive study than the one reported in this communication, requiring the construction and testing of a complete fuel cell stack with integrated reformer. The scope of this study is to provide confirmation of some theoretical benefits and to generate a preliminary guide to the practical benefits and limitations of integrating a reformer into a fuel cell stack.

1.2.1. Simplification of design

Traditional reformed-fuel-fed, low-temperature PEM fuel cell systems are complex. Because of the lack of carbon monoxide tolerance in the fuel cell, the fuel processor is a relatively large, multi-stage device, typically including a reformation reactor, a water-gas shift reactor and a preferential oxidization reactor. Despite the multiple stages, they are known to have occasional instances when the concentration of CO in the fuel cell feed becomes unacceptably high, temporarily poisoning the electrodes and degrading fuel cell performance. In contrast, the internal reforming high temperature PEM fuel cell needs only a single reforming stage because the anode is tolerant of carbon monoxide. The IRFC's reformer is built into the

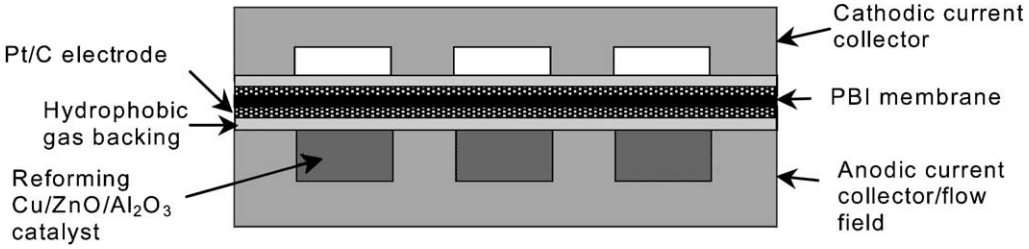

Fig. 2. Drawing of an IRFC cross-section.

anode chamber of the fuel cell, eliminating the need for a separate fuel processor.

1.2.2. Increased overall efficiency

In a traditional reformed-fuel-fed PEM fuel cell, heat is provided to the reformer by burning excess hydrogen from the anode exhaust. This design wastes energy in two ways: (1) fuel that could be used by the fuel cell is instead used to heat the reformer; and (2) excess heat created by the fuel cell is not of high enough temperature to used for useful work and so is usually wasted instead of being used to drive the reformation reaction. In contrast, the IRFC cell does not require the burning of fuel to drive the reforming reaction because it uses the excess heat created by the fuel cell instead. In addition, a heat exchanger is not needed because the reformation catalyst is in direct contact with the heat source.

Thermodynamic calculations confirm that the excess heat created by the operating fuel cell will be sufficient to heat the incoming feed streams as well as provide for the endothermic reformation reaction. For a fuel cell running at 225 °C, −244 kJ of energy is available per mole of H_2 that reacts. Heat capacity calculations show that it would require 17.8 kJ to heat the air containing the 1.5 mol of O_2 necessary for the reaction, leaving 226 kJ of energy left available. Subtracting from this the energy needed to heat and vaporize 1/3 mol of methanol and 1/3 mol of water (32.6 kJ for both) and the heat of reaction needed to reform the reactants (19 kJ), leaves 174.4 kJ still available. Operating the fuel cell at a cell potential of 700 mV, would provide 135 kJ of electrical energy, leaving ca. 39 kJ of heat to be removed from the fuel cell stack to maintain the operating temperature.

1.2.3. Minimization of weight and volume

The mass and volume of the internal reformer fuel cell system is primarily minimized by a combination of the advantages described earlier. Elimination of the water-gas shift and preferential oxidizer reactors in addition to simplification of the reformer design and its integration into the fuel cell would result in a significant decrease in the weight of the fuel processor. Also, an increase in overall fuel efficiency will result in a smaller fuel tank and less fuel mass for the same amount of energy production. However, there is an additional, more subtle, benefit of integrating the reformer into the fuel cell that could result in significant weight loss. Because the reaction rate of the methanol reforming reaction is inversely proportional to the concentration of hydrogen, the rate of methanol conversion is increased when hydrogen is extracted from the reformer. In a standard tube reactor, extraction of the hydrogen from the catalyst bed is difficult. However, when the reformer is integrated into the fuel cell, the anode is located directly above the reforming catalyst bed (see Fig. 2). This configuration creates a hydrogen concentration gradient perpendicular to the flow through the catalyst bed, causing the hydrogen being created in reforming section to diffuse out of the catalyst bed, where it is oxidized at the anode. This results in the overall concentration of hydrogen in the catalyst bed to remain low, accelerating the reforming reaction. The overall mass of the system is reduced because when the reaction rate is faster, less reforming catalyst is needed then in the traditional reformer to achieve the same conversion of methanol.

1.2.4. Inherent dynamic stability

The most efficient low-temperature fuel cell reformer systems combust excess hydrogen from the anode exhaust to heat the reformer. Unfortunately, this configuration is inherently unstable when the fuel cell is driving a dynamic electrical load. Instability arises because the concentration of hydrogen in the anode exhaust is lowest when the electrical load is large and fuel cell requires more hydrogen to maintain the electrical current. Because the concentration of hydrogen in the anode exhaust is low, less heat is provided by the combustion of the anode exhaust to maintain the temperature within the fuel processor, causing rate of hydrogen production and, thus, the current produced by the fuel cell, to drop. In contrast, the IRFC is inherently dynamically stable. As the electrical load on the fuel cell is increased, the heat created by the fuel cell reaction increases as well, and, because the reformer is in direct contact with the fuel cell, this excess heat helps to drive the reforming reaction, creating more hydrogen for the fuel cell instead of less.

1.3. Background

Catalytic steam-reforming of methanol on CuO/ZnO-based catalyst is a process that produces primarily hydrogen and carbon dioxide, but also produces a small amount of carbon monoxide (ca. 1–2%, in the temperature range used in this study). The reactions that are known to occur on this type of catalyst are as follows:

$$CH_3OH + H_2O \underset{k_{-R}}{\overset{k_{+R}}{\rightleftharpoons}} CO_2 + 3H_2 \quad (1)$$

$$CH_3OH \underset{k_{-D}}{\overset{k_{+D}}{\rightleftharpoons}} CO + 2H_2 \quad (2)$$

$$CO + H_2O \underset{k_{-W}}{\overset{k_{+W}}{\rightleftharpoons}} CO_2 + H_2 \quad (3)$$

where Eq. (1) is the reforming reaction, Eq. (2) is the methanol decomposition reaction, and Eq. (3) is the water-gas shift reaction.

In early studies of the methanol-steam reformation reaction, it was thought that methanol initially decomposed to form carbon monoxide and hydrogen, and then the carbon monoxide reacted with water to form carbon dioxide and hydrogen [4]. However, later studies found evidence that contradicted this theory, and instead proposed that methanol reforming occurred by direct reaction with water to produce

carbon dioxide and hydrogen [5]. Due to the complexity of this reaction mechanism, most of the literature examining the methanol-steam reforming reaction has fit the kinetic data to a generalized power rate law expression [5,6]. The power law-based kinetic expression has little theoretical basis, but it is often effective for modeling reaction behavior when the reaction mechanism is unknown or complex. The earliest mechanism-based kinetic model was proposed by Jiang et al. [7]. This model was later expanded by Peppley et al. [8,9], who not only elucidated the role of specific catalytic surface sites, but also included a model for the carbon monoxide production by methanol decomposition and it's consumption by the water-gas-shift reaction. In addition, Peppley et al. verified the applicability of their model by fitting reaction data from a series of kinetic experiments to their model.

Internal steam reforming of methanol in a fuel cell is a concept that was pioneered by Jalen and Giner [10]. Unlike the present study in which a polymer electrolyte membrane fuel cell operating at 225 °C was used, Jalen and Giner attempted to integrate a steam reformer into a phosphoric acid fuel cell (PAFC) that operated at 200 °C. Although this integration was a moderate success, the life of their new device was limited by the tendency of the reforming catalyst to dissolve into the ubiquitous phosphoric acid electrolyte. Even so, they were able to achieve an *iR* corrected potential of 635 mV at 200 mA cm^{-2} with an overall methanol utilization of 64% (80% methanol conversion with 80% H_2 utilization). This result was accomplished with 0.170 g of a CuO/ZnO type catalyst, UCI-G66B, per square centimeter of anode area.

Dissolution of the reforming catalyst into H_3PO_4 is a potential problem not only with PAFCs, but also with the PBI/H_3PO_4-based cells used in this study. Although the severity of the problem is reduced because the total amount of acid and, more importantly, the mobility of the acid in the membrane electrode assembly (MEA) is less in the PBI/H_3PO_4 fuel cell than in a PAFC, the possibility of the H_3PO_4 acid leaching from the MEA into the catalyst bed is still a primary concern. Unfortunately, replacing the catalyst with one that would be tolerant to an acidic environment was not possible because the authors know of no such catalyst that is also both well characterized and capable of steam-reforming methanol at appreciable rates at ca. 225 °C.

To reduce the likelihood of acid leaching from the MEA and into the reforming catalyst bed, E-Tek's ELAT electrodes were used in this study due to their highly hydrophobic gas-backing. It was hoped that during the MEA construction process the hydrophobic gas-backing of these electrodes would help drive the phosphoric acid away from the gas-backing and towards the electrode and membrane, leaving the surface which would be in contact with the reforming catalyst bed relatively acid free. The electrochemical performance of MEAs made from these electrodes was examined in a parallel study, which will be published in the near future [11].

1.4. Objective

The focus of Jalen and Giner's work [10] was to verify the viability of the IRFC concept; and then to quantify the performance of the integrated stack. Unfortunately, the Jalen and Giner study lacked any significant comparison of the reforming reaction rate within the integrated stack to the reforming reaction rate provided by a more idealized reactor configuration, such as would be used for an external reformer. Thus, while they clearly showed that one could build an IRFC, they left it difficult to ascertain whether or not one should build an IRFC. The objective of the present study is to begin to answer that question. By starting with an analysis of the reforming reaction rate within an idealized tube reactor, and then comparing these results with the results from an IRFC reactor, we hope to more clearly delineate, from a system design perspective, the relative advantages, disadvantages, and caveats of integrating the reformer into the fuel cell stack.

2. Experimental

2.1. Experimental apparatus

A schematic of the apparatus used in these experiments is shown in Fig. 3. The fuel tanks of liquid methanol and water were insulated and heated to a temperature of 100 and 138 °C, respectively. These temperatures were chosen in order to maintain the vapor pressure within both feed tanks at approximately 45 psia. From there, the methanol and water vapor were transported through a set of heated lines (165 °C) to the mass flow controller oven that was maintained at 145 °C. After regulation through mass flow controllers (MKS high temperature mass flow controllers, M330AH), the methanol and water vapor were transported through a second set of heated lines (165 °C) and into the reactor oven. Within this oven, the methanol feed, water feed, and non-condensable (He, H_2, CO_2) feed lines were combined through a cross-type union into a single line and fed to a small (ca. 20 cm^3) mixing tank and then to the reactor. Flow rates of the non-condensable gases were regulated using MKS 1359c mass flow controllers. In order to ensure that all the feed gases attained thermal equilibrium with the reactor oven before entering the reactor, all feed lines in the reactor oven were constructed of 1/8 in. o.d. copper and were a minimum of two meters in length. Upon exiting the reactor, the reaction products, as well as unreacted methanol and water, flowed through a line that exited the reactor oven and fed directly into a Pyrex vacuum trap, which was maintained at 0 °C by immersion in ice water. The predominance of unreacted methanol and water thus removed, the flow rate of reaction products was then measured using a vapor flow meter (J&W Scientific, ADM2000).

For experiments that required the IRFC, the experimental apparatus was changed only by removing the isothermal tube reactor and inserting the IRFC in its place.

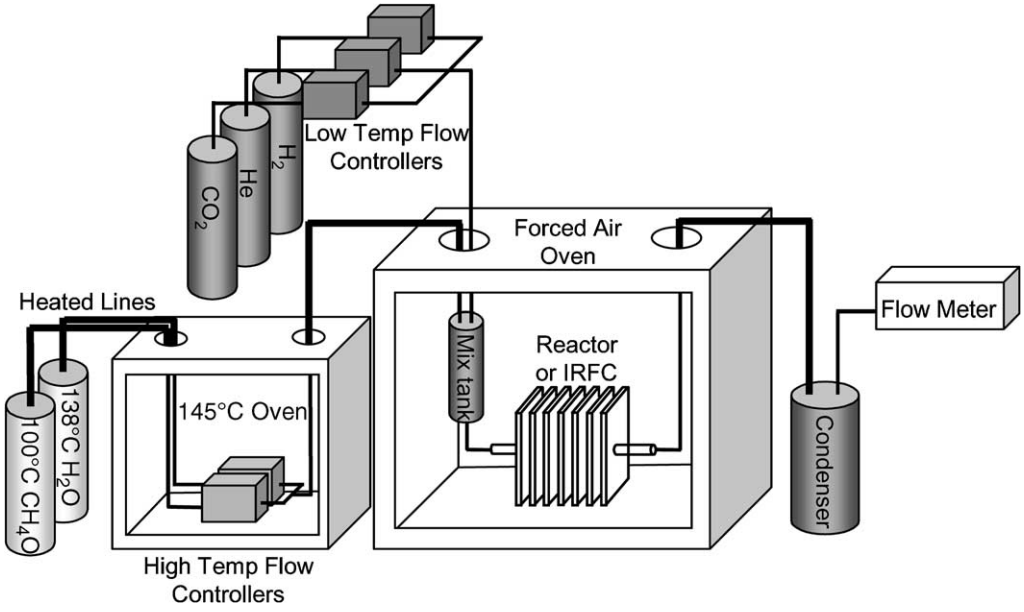

Fig. 3. Schematic of experimental apparatus used for tube reactor experiments as well as IRFC experiments.

2.2. Membrane electrode assembly (MEA) preparation

The polybenzimidazole (PBI) films were cast with H_3PO_4, using trifloroacetic acid (TFA) as solvent. A detailed description of membrane preparation procedure has been published previously [12]. The thickness of the membranes was typically 0.075 mm (3 mil) and the acid content of the membranes was approximately six H_3PO_4 molecules per repeat unit in the polymer. Electrodes were obtained from E-Tek (Natick, MA, USA) and were the standard single sided ELAT type (20% Pt on XC-72, 0.35 mg Pt cm^{-2} on a hydrophobic gas-backing).

All MEAs used in these experiments were constructed using the following procedure. The PBI membrane was first dried under vacuum at 95 °C for 1 h. The ELAT electrodes were soaked in a solution made from one part 5 M H_3PO_4 and seven parts ethanol by volume for 5 min after which they were removed from solution and dried in an oven at 120 °C for 15 min. The acid containing electrodes were then pressed onto the membrane for 5 min at a temperature of 150 °C and a pressure of 1.78×10^7 N m^{-2} (400 lbsf cm^{-2}).

2.3. Isothermal tube reactor

The isothermal tube reactor (shown in Fig. 4) was constructed using a 10 cm long stainless steel tube (0.175 cm i.d., 0.318 cm o.d.) with copper fins attached to the tube with silver solder. The 16 copper fins (each 0.08 cm thick,

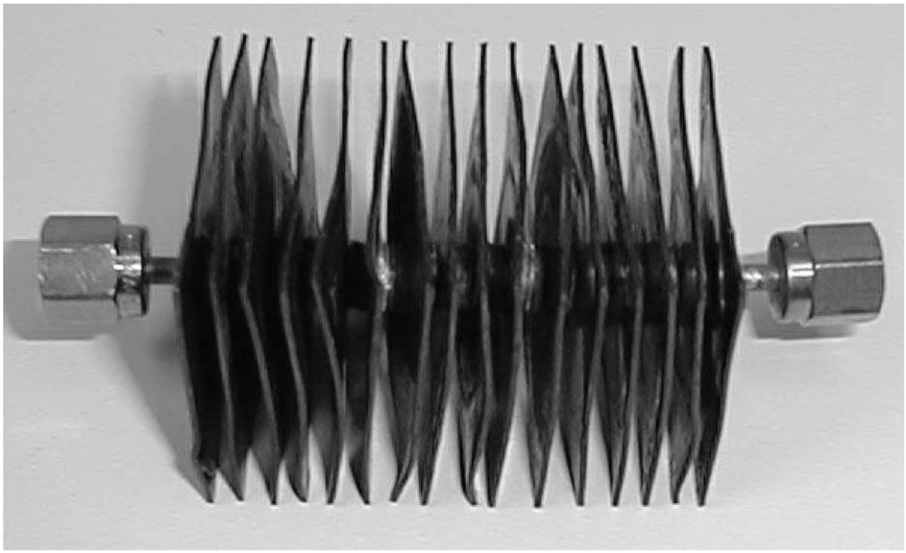

Fig. 4. Photograph of the copper finned tube reactor.

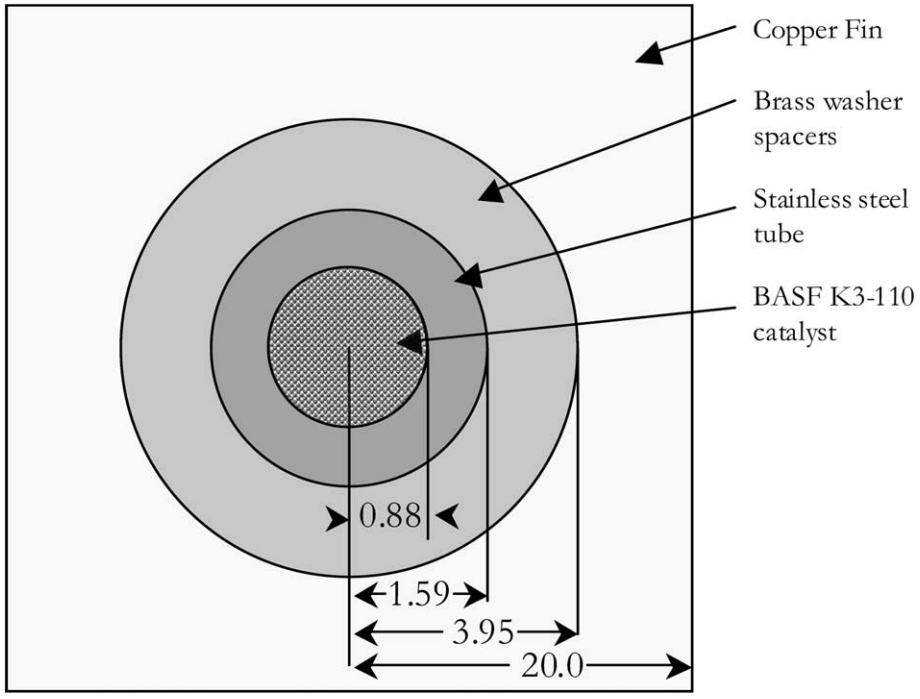

Fig. 5. Drawing of isothermal tube reactor cross-section. All measurements are in millimeters.

3.8 cm × 3.8 cm) were fixed uniformly along the center 6 cm of the reactor. During construction and before soldering, the gaps between the copper fins were maintained by brass washers (0.32 cm i.d., 0.79 cm o.d.), which were placed between each copper fin. When the reactor was soldered, the copper washers fused together with the copper fins and the stainless steal tube, creating a single structure. A cross-sectional drawing of the tube reactor is shown in Fig. 5. The reforming catalyst was held in the center most section of the tube reactor using glass wool plugs. In order to ensure a high thermal transfer rate, the catalyst bed was limited to the center 6 cm of the reactor, where the copper fins were located. This effectively limited the capacity of the reactor to a maximum of 0.14 g of the BASF K3-110 catalyst used in this study.

The copper fins were soldered onto the tube and the reactor was operated in a forced convection oven in order to ensure isothermal operation. With this design, the reactor remained as simple as possible with no thermocouple ports or other complicating devices. Estimation of the reactor's effective heat transfer coefficient was calculated using a semi-empirical model [13]. These calculations concluded that the greatest temperature drop between the oven temperature and the temperature within the tube would be less than 1 °C for all of the experimental runs. Thus, the reactor could be considered isothermal.

2.4. Internal reforming fuel cell

Fig. 6 is a photograph of the primary components of the IRFC. The components shown in this picture are, from left to right, the aluminum anode end plate, the stainless steel anode current collector, the stainless steel cathode current collector, and the aluminum cathode end plate. Not shown in this picture, but necessary for proper operation, are: a glass fiber supported Teflon gasket which provides electrical isolation between the cathode current collector and the cathode end plate; the E-Tek electrodes on PBI MEA, which separates the anode and the cathode current collecting plates; and two glass fiber supported Teflon gaskets, which were used on either side of the MEA for structural support of the PBI membrane. The aluminum end plates were constructed identically except for a 1/4 in. hole that was drilled through the anode backing plate parallel to the plane of the MEA. This hole can be seen in the lower left-hand side of the picture, just above the anodic feed port. Before operation, a pencil shaped cartridge heater was inserted into this hole. During operation, power was applied to the cartridge heater by a controller that measured the temperature of the anode via a thermocouple placed in a small groove behind the anodic current collector plate. This heater effectively eliminated the need for a large heat transfer coefficient between the metal of the IRFC and the surrounding air and maintained the temperature of the reforming reactor bed during reforming.

The reactor bed in the anode current collector plate was designed to be as close as possible to the plug flow geometry of the isothermal reactor. The S-shaped channel had an effective length of 5.75 cm, a depth of 0.081 cm, and a width of 0.307 cm, making a cross-sectional area of 0.025 cm^2. This compares well with the geometry of the tube reactor, which had a length of 6.0 cm and a cross-sectional area of

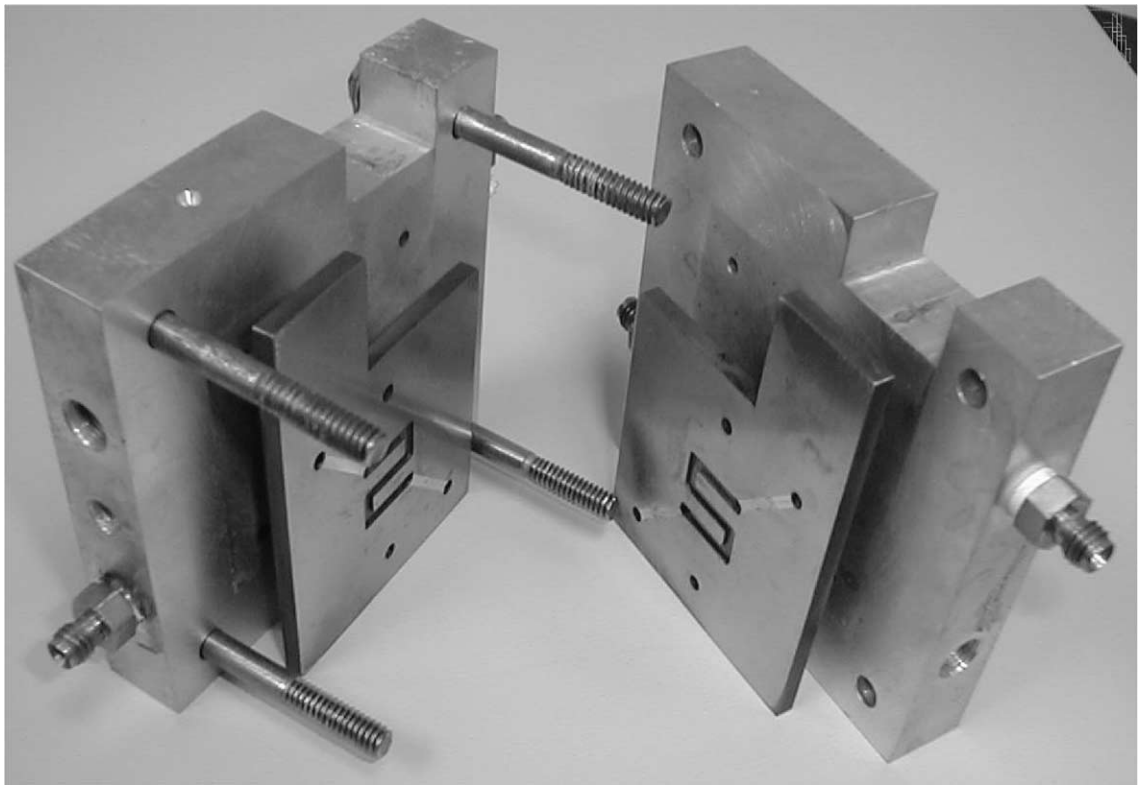

Fig. 6. Photograph of the primary pieces of the internal reforming fuel cell hardware.

0.024 cm^2. During operation, the catalyst was held in place by the anodic electrode and by carbon-felt plugs placed at the beginning and the end the S-shaped catalyst bed.

2.5. Catalyst and reagents

The catalyst used for reforming in this study was the low-temperature shifts catalyst BASF K3-110, the composition of which is 40/40/20 wt.% $CuO/ZnO/Al_2O_3$. As received, the catalyst was in pellet form with each pellet being far too large to use in our reactor setup. To address this, the pellets were milled for several hours and then sifted. All of the catalyst used in this study consisted of particles between 155 and 170 μm in diameter. The physical characteristics of BASF K3-110, as reported in the literature, are shown in Table 1. The reagents used in this study were as follows: the methanol was obtained from Fisher (spectroscopic grade), the water was deionized using a Nanopure II deionizer, and all non-condensable gases (He, H_2, CO_2, O_2) were industrial grade.

Table 1
Physical characteristics of BASF K3-110 catalyst (from Peppley et al. [9])

Characteristic	Value
CuO (wt.%)	40
ZnO (wt.%)	40
Al_2O_3 (wt.%)	20
Nitrogen BET area ($m^2\ g^{-1}$)	102 ± 4
Pore volume (ml g^{-1})	0.35
Copper area ($m^2\ g^{-1}$)	9.83
Dispersion (%)	4.8
Copper crystallite size (Å)	219

2.6. Calibration procedure

The ADM2000 gas flow meter was calibrated as received using NIST standards. The MKS 1359c mass flow controllers were calibrated using the ADM2000.

The high temperature water and methanol vapor mass flow controllers were calibrated as follows. With the tube reactor loaded with the catalyst and placed in line, and the reactor oven at operating temperature (225 °C) the ADM2000 was used to measure the flow of N_2 through each high temperature mass flow controller. The gas correction factors to correlate between N_2 and water, and N_2 and methanol were then obtained by flowing pure water and methanol through their corresponding mass flow controller for a period of 24 h and condensing the vapor stream in the vacuum trap, which was maintained at 0 °C. The volume of liquid collected was then measured, and the actual molar flow rate of methanol or water was compared with the nitrogen flow rate that had been measured previously. Using this procedure, the gas correction factors of methanol and water at 145 °C were found to be 0.507 and 0.821, respectively. Thus, when calibrating the mass flow controllers using N_2 gas, one needs to multiply by 0.507 to obtain

the true methanol flow rate, and by 0.821 to obtain the true water flow rate. This is noted here only because these values differ slightly from the gas correction factors calculated for methanol and water using the standard procedure, which is outlined in any mass flow controller manual.

Due to the unavailability of a suitable high temperature pressure gauge, the pressure drop across the reactor was not measured during reforming. To estimate the pressure drop, the tube reactor was loaded with the reforming catalyst and placed in line. Room temperature N_2 was then passed through the reactor, and the pressure drop measured versus the N_2 flow rate. This pressure drop curve was then correlated with the experimental data by assuming that the flow rate of products exiting the operating reactor correlated with the flow rate of N_2 used during calibration. For example, if it was found during the calibration that 50 sccm of N_2 produced a pressure drop of 5 psi, it was assumed that if, during steam reforming, the reactor produced 50 sccm of products, the pressure drop across reactor would also be approximately 5 psi.

2.7. Experimental procedure

The kinetic experiments using the tube reactor were conducted as follows. The catalyst was weighed out and funneled into the reactor using a glass pipette. The loaded reactor was then placed in line within the reactor oven of the testing apparatus. Helium gas was then passed through the reactor while the temperature of the reactor oven was raised to 225 °C. When thermal equilibrium was achieved, the helium flow was shut off, and a flow of 12.7 sccm water vapor and 9.4 sccm methanol vapor was passed through the reactor for 24 h. This conditioning period was necessary to allow the copper oxide and zinc oxide to reach equilibrium with their respective metals in the reductive atmosphere. To ensure that the catalyst had reached equilibrium, the conversion rate was tracked for a subsequent 6 h. If the reaction rate was found to be stable, experiments were commenced. The kinetic experiments were often conducted over a matter of days, so to ensure a constant catalyst activity, the reaction rate was measured at the beginning and at the end of each day using the same feed rates and temperature as was used for the conditioning procedure. This periodic check was also used to verify reproducibility of the data.

The experimental procedure for the IRFC experiments were conducted in a similar fashion. The catalyst was first weighed out and then placed into the S-shaped reactor bed in the anode current collector. The MEA was then placed above the catalyst bed, and the remaining pieces of the IRFC were put in place and bolted together. The cell was then placed in line in the reactor oven and helium was passed through the cell while the temperature of the oven was raised to 225 °C. The initial conditioning routine for the catalyst was done using the same method as described earlier for the tube reactor, as were the periodic activity checks that were performed at the beginning and end of each day.

Individual experimental runs were conducted as follows. Flow rates of the feed gases (water, methanol, and H_2, CO_2, He) were set using the mass flow controllers. The reactor was then given 5–10 min to reach equilibrium (lower feed rates were allowed 10 min) after which time the mass flow rate of non-condensable vapors exiting the reactor was measured using the ADM2000. Because this flow rate had a tendency to fluctuate over time, the ADM2000 was used to sample the flow rate 400 times in a time span of approximately 5 min and the average of these samples was used. After the flow rate was measured, the feed flow rates were then adjusted, and the process repeated for the next data point.

3. Results and discussion

This section is segmented into Sections 3.1–3.3, reflecting the experimental and analytical process taken for this study. Section 3.1 deals with the results obtained from the isothermal tube reactor. Section 3.2 is dedicated to the subsequent selection of a model and fitting of the data to obtain a kinetic expression. Section 3.3 focuses on the results obtained from the IRFC and analyzing these results using the kinetic expression.

3.1. Kinetic data from the isothermal tube reactor

It is often a characteristic of surface catalyzed heterogeneous reactions that the kinetic expression obtained using a particular set of operational parameters is not suitable to accurately predict reactor behavior using a different set of operational parameters. In particular, the reaction rate on high surface area catalysts, like the one used in this study, can be highly dependent upon the velocity of material moving through the reactor. In this situation, when transport related factors are experimentally inseparable from kinetic factors, the expression obtained is not a true kinetic expression, but can be thought of instead as an effective kinetic expression. So, although many previous papers on methanol-steam reformation included a kinetic expression for predicting reaction behavior (some even using the same BASF K3-110 catalyst), it was still necessary to determine an effective kinetic expression for the reaction under conditions similar to those that would exist in the IRFC.

It was for this same reason that the cross-sectional area and average length of the reforming catalyst bed in the IRFC was made to be the same as the cross-sectional area and length of the catalyst bed in the isothermal tube reactor. Thus, reaction rate data and the resulting effective kinetic expression obtained using the isothermal tube reactor could be directly compared with reaction rate data obtained from the IRFC. Any differences could then be attributed to the effect of the hydrogen-extracting anode present in the IRFC. So, while many kinetic studies employ so-called differential reactors in an effort to minimize error due to

Table 2
Limits of operating parameters used during kinetic experiments with the PFR

Variable	Temperature (°C)	Inlet pressure (atm)	Apparent space-time (s)	Water/MeOH molar feed ratio	H_2 in feed (%)	CO_2 in feed (%)	He in feed (%)	MeOH conversion (%)
Low	225	1.06	0.034	1.16	0.0	0.0	0.0	27.5
High	250	1.65	0.65	5.15	54.4	50.6	57.3	100.0

diffusion-mixing effects, the reactor used in this study was a fixed bed tube reactor. This type of reactor is also known as an integral reactor due to the necessity of integrating the rate expression over the volume of the reactor (or total mass of catalyst) in order to properly analyze experimental results.

The limits of the operating parameters used in the 70 kinetic experiments performed using the isothermal tube reactor are shown in Table 2. The inlet pressure listed in this table, as explained in the previous section, is an estimate of the pressure drop that developed across the reactor bed due to the flow of vapor through the restriction of the catalyst bed. The outlet from the reactor was unobstructed, aside from the condenser and the digital flow meter, which were assumed to contribute negligible pressure drop. Thus, the outlet pressure was assumed to be 1 atm. Calculation of the apparent space-time for gases in the reactor was done using the inlet flow rates and the empty volume of the reactor (as opposed to the actual vapor volume in the reactor). The feed ratio of water to methanol was maintained above 1.1 in order to minimize the possibility of coking (the formation of solid carbon as a byproduct of the reaction). The methanol conversion varied from 27% at the maximum flow rate to nearly complete conversion.

As discussed in the Section 2, the reactor was checked periodically at a standard temperature and feed condition to confirm that the activity of the catalyst was sufficiently stable during the series of kinetic experiments. A graph showing the normalized reactor H_2 output obtained during these checks versus time appears in Fig. 7. As this figure shows, during the approximately 44 h in which data was taken, the H_2 output of the reactor dropped only ca. 4%. This was considered small enough of a drop to be within the range of experimental error, and thus, no attempt was made to correct for the slight change in catalyst activity.

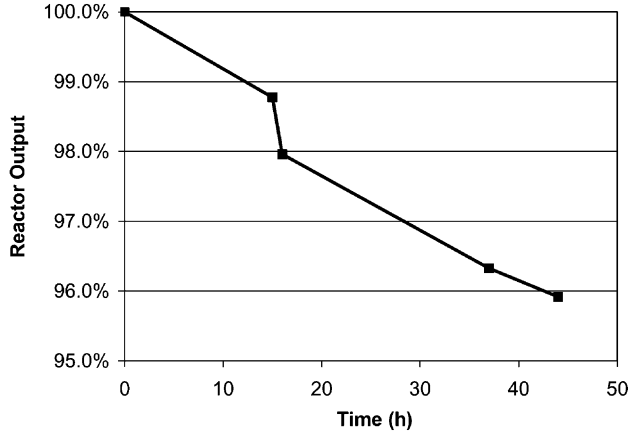

Fig. 7. Normalized H_2 output of the tube reactor at a specific temperature feed rate, and feed composition over the time period in which kinetic data was taken.

3.2. Determination of the kinetic expression

For any chemical reaction, the overall reaction rate under any given inlet condition (assuming no mass or heat transfer effects) is a function of three factors: the reaction stoichiometry, which is mathematically described by the mass balance equations; the configuration of the reactor, which is mathematically described by the design equation; and the inherent reaction mechanism, which is mathematically described by the kinetic expression (also known as the rate law).

The first of these, the mass balance equations, are as follows for the vapor phase reforming reaction (ignoring CO production):

$$p_j = P\frac{F_j}{F_\mathrm{M} + F_\mathrm{W} + F_\mathrm{H} + F_\mathrm{C} + F_\mathrm{I}} \tag{4}$$

$$F_\mathrm{M} = F_{\mathrm{M}0}(1 - X), \qquad F_\mathrm{W} = F_{\mathrm{W}0} - F_{\mathrm{M}0}X,$$
$$F_\mathrm{H} = F_{\mathrm{H}0} + 3F_{\mathrm{M}0}X, \qquad F_\mathrm{C} = F_{\mathrm{C}0} + F_{\mathrm{M}0}X,$$
$$F_\mathrm{I} = F_{\mathrm{I}0} \tag{5}$$

where p_j is the partial pressure of any component, P the total pressure in the reactor, F the molar flow rate, X the dimensionless conversion of methanol, and the subscripts M, W, H, C, and I refer to methanol, water, hydrogen, carbon dioxide and inert, respectively, and the subscript 0 refers to the feed condition. The rate of CO production was assumed to be negligible for these conditions.

Design equations are well known for any idealized type of reactor and are readily available from the literature. For the tube reactor used in this study the design equation for a PFR was used, given as

$$F_{\mathrm{M}0}\frac{\mathrm{d}X}{\mathrm{d}m} = -r'_\mathrm{M} \tag{6}$$

where $F_{\mathrm{M}0}$ is the molar flow rate of methanol in the feed, X the dimensionless conversion of methanol, m the mass of catalyst, and r'_M is the rate of methanol conversion per unit mass of catalyst.

The final crucial factor, the kinetic expression, is specific to the catalyst and to the reaction mechanism, and is

frequently unknown. As such, it may be either guessed, using a general mathematical expression, or deduced, using intimate knowledge of the reaction mechanism.

Because the focus the present study was to examine the viability of, as well as the effects of integrating the reformer into the fuel cell and not an examination of the reforming reaction itself, a thorough and fundamental understanding of the mechanisms of the methanol-steam reforming reaction (as well as side reactions) was not pursued. In this situation, it is common to use a purely empirically-based kinetic expression, such as the so-called power law-based expressions that are frequently found in kinetics literature. That being said, this study does require a mathematical model that can accurately predict the effect of hydrogen concentration on the overall reaction rate. Hydrogen concentration effects are of particular interest because drawing current from the IRFC removes hydrogen from the reforming catalyst bed. It was thought that a fundamental, surface-mechanism-based kinetic model would most accurately predict the effect of hydrogen concentration on reaction rate. Unfortunately, this is not always the case. Because transport effects can have a significant impact on the apparent kinetics of a high surface area catalyst such as BASF K3-110, the ironic result is that sometimes an empirically-based kinetic expression can actually predict the overall reaction rate in a specific reactor more accurately than a mechanism-based kinetic expression. In this situation, the kinetic expression obtained should not be considered the true kinetic expression because it is limited in its application, but it can be considered an effective kinetic expression that holds for a given range of temperatures, feed rates, and feed compositions. For this reason, the kinetic data obtained from the isothermal tube reactor was fit to both the mechanism-based kinetic expression of Peppley et al. [8] as well as to a power law kinetic expression.

3.2.1. Fit using a mechanism-based kinetic expression

As discussed in Section 1, the steam-reforming model developed by Peppley et al. [8] included not only a mechanism-based kinetic expression for the methanol reforming reaction (Eq. (1)) on $CuO/ZnO/Al_2O_3$ catalyst, but also expressions for the decomposition of methanol (Eq. (2)) and the water-gas shift reaction (Eq. (3)). However, the present study does not concern itself with the production of CO, and so only Peppley's kinetic expression for the methanol reforming reaction was used for the fitting of the tube reactor data. Although, in theory, this omission does introduce some error, the actual error should be insignificant because, at these temperatures, the rate of CO production is small as compared to the rate of reforming.

The kinetic expression for methanol reforming, as developed by Peppley et al. is of the form:

$$-r'_{\mathrm{M}} = S_{\mathrm{A}} \frac{k_{\mathrm{R}} K^*_{\mathrm{CH_3O}} (p_{\mathrm{M}}/p_{\mathrm{H}}^{1/2})(1 - p_{\mathrm{H}}^3 p_{\mathrm{C}}/K_{\mathrm{R}} p_{\mathrm{M}} p_{\mathrm{W}}) C^{\mathrm{T}}_{\mathrm{S_1}} C^{\mathrm{T}}_{\mathrm{S_{1a}}}}{(1 + K^*_{\mathrm{CH_3O}}(p_{\mathrm{M}}/p_{\mathrm{H}}^{1/2}) + K^*_{\mathrm{HCOO}} p_{\mathrm{C}} p_{\mathrm{H}}^{1/2} + K^*_{\mathrm{OH}}(p_{\mathrm{W}}/p_{\mathrm{H}}^{1/2}))(1 + K_{\mathrm{H}}^{1/2} p_{\mathrm{H}}^{1/2})} \tag{7}$$

where S_{A} is the surface area of catalyst per mass, and $C^{\mathrm{T}}_{\mathrm{S1}}$ and $C^{\mathrm{T}}_{\mathrm{S1a}}$ are surface concentrations of adsorption sites. The remaining variables in Eq. (7) are defined as follows:

$$k_{\mathrm{R}} = k_{\mathrm{R}}^{\infty} \exp\left(-\frac{E_{\mathrm{R}}}{RT}\right) \tag{8}$$

$$K_{\mathrm{R}} = \exp\left(\frac{\Delta S_{\mathrm{R}}}{R} - \frac{\Delta H_{\mathrm{R}}}{RT}\right) \tag{9}$$

$$K^*_{\mathrm{CH_3O}} = \exp\left(\frac{\Delta S^*_{\mathrm{CH_3O}}}{R} - \frac{\Delta H^*_{\mathrm{CH_3O}}}{RT}\right) \tag{10}$$

$$K^*_{\mathrm{HCOO}} = \exp\left(\frac{\Delta S^*_{\mathrm{HCOO}}}{R} - \frac{\Delta H^*_{\mathrm{HCOO}}}{RT}\right) \tag{11}$$

$$K^*_{\mathrm{OH}} = \exp\left(\frac{\Delta S^*_{\mathrm{OH}}}{R} - \frac{\Delta H^*_{\mathrm{OH}}}{RT}\right) \tag{12}$$

$$K_{\mathrm{H}} = \exp\left(\frac{\Delta S_{\mathrm{H}}}{R} - \frac{\Delta H_{\mathrm{H}}}{RT}\right) \tag{13}$$

Thus, the predicted conversion rate is solved by combining the mass balance equations (Eqs. (4) and (5)) with the design equation (Eq. (6)), and with the kinetic expression (Eq. (7)); and then integrating from a catalyst mass of zero to the total catalyst mass in the reactor, m. To find the best fit for the kinetic data, the reforming reaction portion of Peppley's model (shown earlier) presents a total of twelve adjustable parameters, k_{R}^{∞}, E_{R}, ΔS_{R}, ΔH_{R}, $\Delta S^*_{\mathrm{CH_3O}}$, $\Delta H^*_{\mathrm{CH_3O}}$, $\Delta S^*_{\mathrm{HCOO}}$, $\Delta H^*_{\mathrm{HCOO}}$, ΔS^*_{OH}, ΔH^*_{OH}, ΔS_{H}, and ΔH_{H}. As recommended in Peppley's paper, the fitting process was simplified by fixing six of these parameters to values found in the literature. The remaining six parameters were then adjusted to fit the data by minimizing the squared sum of the error between the actual conversion and the predicted conversion. The value of the parameters found for the optimal fit are listed in Table 3, in which values that were fixed to values from the literature are in italics.

For the 70 experimental runs used in the fitting, the average magnitude of error between the predicted conversion, using the model given earlier, and the experimentally measured conversion was calculated to be 5.6% with a standard deviation of 4.5%; the error being defined as $(X_{\mathrm{measured}} - X_{\mathrm{predicted}})/X_{\mathrm{measured}}$. In addition, 59 of these runs had a prediction error of less than ±10% and all were within ±18%. A plot showing the rate of methanol conversion predicted by Peppley's mechanism-based model versus the actual rate of methanol conversion for the 70 experiments appears in Fig. 8. This figure demonstrates that the Peppley's reforming model is sufficient for estimating conversion for methanol conversion rates from ca. 0.01 to 0.15 mol s^{-1} $kg^{-1}_{\mathrm{catalyst}}$.

In order to help verify that the conversion errors predicted by the Peppley's model do not correlate with a particular

Table 3
Value of parameters used in least squares fitting of kinetic data from the PFR to Peppley's model[a]

Rate constant or equilibrium constant	ΔS_i (J mol^{-1} K^{-1}) or k_R^∞ (m^2 s^{-1} mol^{-1})	ΔH_i (kJ mol^{-1}) or E (kJ mol^{-1})
k_R^∞ (m^2 s^{-1} mol^{-1})	7.75E+16	122.4
K_R (bar^2)	*88.1*	*25.5*
$K^*_{CH_3O}$ (bar$^{-0.5}$)	−30.9	*−20.0*
K^*_{HCOO} (bar$^{-1.5}$)	210.7	*100.0*
K^*_{OH} (bar$^{-0.5}$)	−174.6	*−20.0*
K_H (bar$^{-0.5}$)	−104.2	*−50.0*

[a] Values in italics were fixed during the fitting, being set to values found in the literature [9].

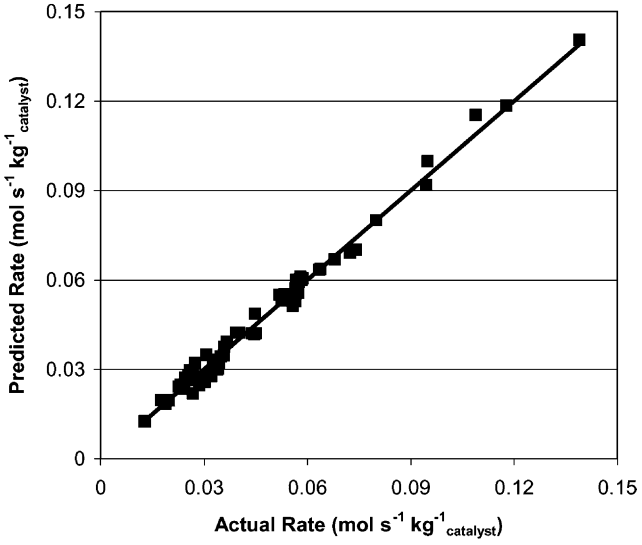

Fig. 8. Rate of methanol conversion as predicted by the Peppley's mechanism-based model vs. the actual rate of methanol conversion for the 70 experimental data points used in the least squares fit.

experimental parameter, an analysis was performed in which the errors were evaluated as a function of several experimental parameters. For example, all of the experimental runs in which H_2 was added to the feed were grouped together and the magnitude of the error in conversion predicted by Peppley's model for each point in this group were averaged together. The results from this analysis appear in Table 4. This table shows that the greatest error in the Peppley's model occurs when H_2 is present in the feed. However, the average magnitude of error in this category is still less than 10%. Aside from this, the remainder of Table 5 is as expected: the general trend being greater relative error when a greater number of mass flow controllers were used (to feed the non-condensable). The larger average errors at 225 and 240 °C than at 250 °C are likely because the lower temperature experiments were conducted first, when the catalyst was more likely to be in the process of achieving steady state.

3.2.2. Fit using a power law-based kinetic expression

The general form of the power law expression used to fit the kinetic data was of the form:

$$-r'_M = A \exp\left(-\frac{E_a}{RT}\right) p_M^\alpha p_W^\beta p_H^\gamma p_C^\eta \quad (14)$$

where A is the pre-exponential factor (sometimes referred to as the frequency factor), E_a the energy of activation, R the universal gas constant, T the temperature, and p_j is the partial pressure of component j. The subscripts, M, W, H, and C refer to the primary reactants and products, methanol, water, hydrogen, and carbon dioxide, respectively. The four exponents, α, β, γ, and η, are unknown, and along with the pre-exponential, A, and the activation energy, E_a, comprise the six parameters to which the least squares fitting of the kinetic data is performed. The non-linear least squares fit resulted in the following kinetic expression:

$$-r'_M = 6370 \exp\left(-\frac{74,164}{RT}\right) p_M^{0.63} p_W^{0.39} p_H^{-0.23} p_C^{-0.07} \quad (15)$$

where the unit of r'_M is mol s^{-1} g$^{-1}_{catalyst}$, the unit of E_a is J mol^{-1} K^{-1}, and the partial pressures have unit of atm, resulting in the units of A (the pre-exponential) to be mol s^{-1} atm$^{-0.72}$.

Table 4
Average error in the methanol conversion predicted by the Peppley's mechanism-based kinetic expression under different experimental conditions

H_2 in feed (%)	CO_2 in feed (%)	He in feed (%)	Water to methanol ratio <1.5 (%)	Water to methanol ratio >1.5 (%)	High space-time (%)	Low space-time (%)	225 °C (%)	240 °C (%)	250 °C (%)
9.9	7.5	8.0	4.7	6.3	2.1	6.6	6.8	6.4	2.8

Table 5
Average error in the methanol conversion predicted by the power law-based kinetic expression under different experimental conditions

H_2 in feed (%)	CO_2 in feed (%)	He in feed (%)	Water to methanol ratio <1.5 (%)	Water to methanol ratio >1.5 (%)	High space-time (%)	Low space-time (%)	225 °C (%)	240 °C (%)	250 °C (%)
9.6	5.2	5.8	4.5	5.7	1.8	6.1	6.2	5.7	3.0

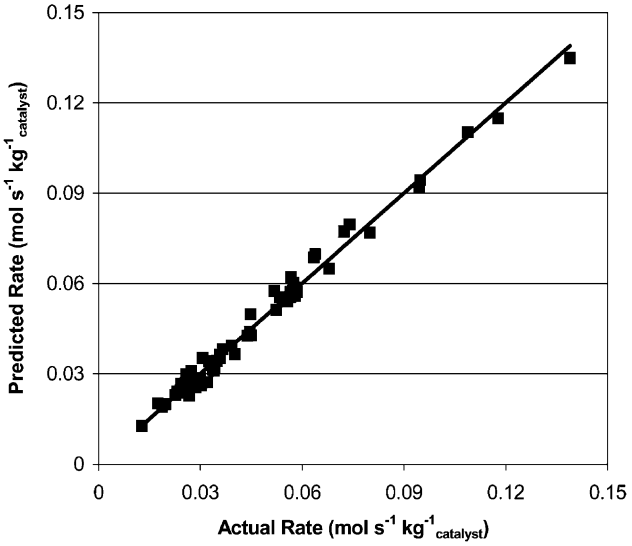

Fig. 9. Rate of methanol conversion as predicted by the power law model vs. the actual rate of methanol conversion for the 70 PFR experimental data points used in the least squares fit.

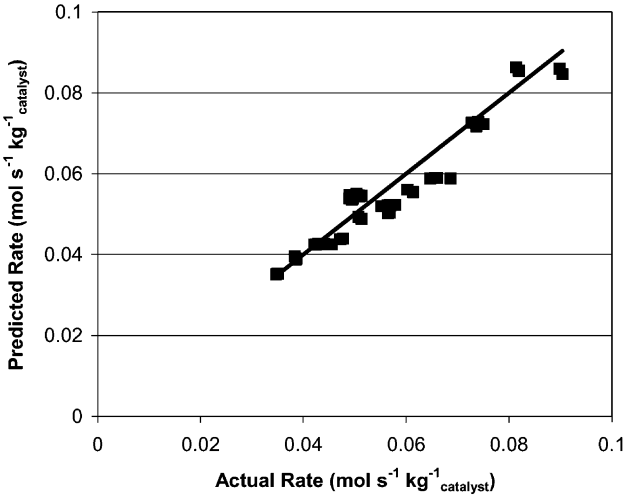

Fig. 10. Rate of methanol conversion as predicted by the Peppley's mechanism-based model vs. the actual rate of methanol conversion for a set of PFR experiments not used in the least squares fit.

For the 70 experimental runs used in the fitting, the average magnitude of error between the predicted conversion and the experimentally measured conversion was calculated to be 5.2% and the standard deviation was 4.5%; the error being defined as $(X_{\text{measured}} - X_{\text{predicted}})/X_{\text{measured}}$. In addition, 58 of these runs had a prediction error of less than ±10% and all were within ±16%. A plot showing the rate of methanol conversion predicted by the earlier power law model versus the actual rate of methanol conversion for the 70 experiments appears in Fig. 9. This figure demonstrates that the power law model is sufficient for estimating conversion for methanol conversion rates from ca. 0.01 to 0.15 mol s^{-1} $kg^{-1}_{\text{catalyst}}$.

As with the error results from Peppley's model, the errors from the power law model were evaluated as a function of several experimental parameters. The results from this analysis appear in Table 5. As with the previous results, this table shows that the greatest error in the power law model occurs when H_2 is present in the feed. However, the average magnitude of error in this category is still less than 10%. As with the error results from Peppley's model, the other entries of Table 5 are as expected. A greater relative error was observed when non-condensable were fed and at the lower temperatures when the catalyst was still in the process of achieving steady state.

Comparison of the error in prediction given by the Peppley's model shown in Table 4 with that given by the power law model shown in Table 5 reveals that there is not a significant difference between the fit provided by either model. Thus, either of these models would be adequate for purposes of this study. However, because the Peppley's model is based on intimate knowledge of the reaction mechanism while the power law model is not, there is reason to believe that Peppley's model will more accurately predict reaction behaviors outside the realm of the parameters space used for the tube reactor kinetic experiments. For this reason, Peppley's model with the estimated parameters listed previously was used for kinetic calculations in the remainder of this communication.

To further verify the kinetic model as well as to test the reproducibility of the tube reactor data, the predicted conversion of methanol was calculated for a number of experiments that were run previously during the setup and testing of the experimental apparatus. Fig. 10 displays a plot of the rate of methanol conversion predicted for an ideal PFR using Peppley's kinetic model versus the actual rate of methanol conversion for those runs. This plot demonstrates that the model can effectively predict methanol conversion, and that the data collected from the tube reactor are reproducible.

3.3. Results from the internal reforming fuel cell

With a suitable model for the kinetic expression obtained, an analysis was done of the effects of integrating the reformer into the anode chamber of the IRFC. The first effect that must be taken into account is the change in geometry of the reactor. As discussed in Section 2, the cross-sectional area and the (average) length of the reactor bed in the IRFC were designed to be the same as the cross-sectional area and length of the reactor bed in the tube reactor. This was to help insure that the gas velocity as well as the residence time in both reactors would be the identical. However, despite these efforts to minimize differences, the two reactor beds are not identical. The cross-section of the tube reactor is circular, where as the cross-section of the IRFC reactor bed is rectangular. Also, the IRFC reactor bed is S-shaped, whereas the tube reactor bed was straight. More significantly, the "ceiling" of the IRFC reactor bed is the fuel cell anode backing (see Fig. 2) which is essentially a porous carbon cloth. This could allow a significant amount of the vapor in the reactor bed to bypass the reforming

catalyst by flowing parallel to the plane of the electrode through the anode backing. These design compromises in the IRFC reactor bed have the effect of increasing the potential for channeling, mixing, and bypassing to occur: all of which would reduce the overall effectiveness of the reactor.

3.3.1. Methanol conversion in the IRFC without an MEA

In order to evaluate the effect of the IRFC reactor bed's non-ideality, the IRFC was put together in the normal fashion except that in place of the MEA, an as received ELAT electrode (without H_3PO_4 loading) and a thin (100 μm) stainless steel sheet were inserted. This configuration simulated the non-ideal geometry as well as the porous carbon ''ceiling'' without introducing added complications (such as the presence of H_3PO_4 as well as possible H_2 diffusion through the polymer electrolyte) inherent when using a PBI/H_3PO_4-based MEA. Once constructed, the IRFC was placed in the testing oven, and the catalyst was given the identical pretreatment that had been given the catalyst in earlier experiments with the tube reactor. Results from these experiments are plotted in Fig. 11 as predicted rate of methanol conversion versus the experimentally measured conversion. The black squares in this figure represent the predicted conversion rate using 0.136 g of catalyst, which was the true mass of catalyst in the IRFC reactor bed. It is clear that the methanol conversion predicted for these experiments is consistently greater than the actual conversion measured: an indication that there is a significant amount of non-ideality in the IRFC reactor configuration. In order to compensate for this, the kinetic model was adjusted by reducing the mass of catalyst to an effective 0.080 g. The resulting predicted conversions are plotted as the gray squares in Fig. 11. The predicted conversion is now consistent with the experimental values. This indicates that, due to deviations from ideal plug flow, the IRFC reactor loaded with 0.136 g of catalyst behaves like an ideal PFR loaded with only 0.080 g of catalyst (58.8% of actual catalyst mass).

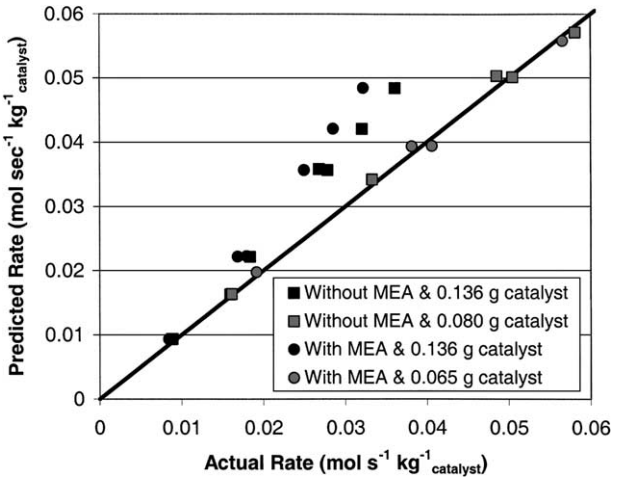

Fig. 11. Rate of methanol conversion as predicted by the Peppley's kinetic model using the true catalyst mass of 0.136 g (black points), as well as a reduced catalyst mass to take into account reactor non-ideality (gray points) vs. the actual rate of methanol conversion in the IRFC with (gray and black circles) and without (gray and black squares) the MEA.

Using an effective catalyst mass of 0.08 g versus the actual mass of 0.136 g is only one of the ways in which the non-ideality of the reactor can be taken into account. Other ways of introducing non-ideality, such as treating the reactor as a PFR in parallel with an ideal mix tank reactor, or simply including a bypass for a certain percentage of the feed, were explored as well. In particular, the model representing a PFR in parallel with a bypass fit the data well at the higher flow rates. The bypass model indicated that, at high feed rates, approximately 35% of the flow bypassed the catalyst bed completely. Presumably, this bypass flow paralleled the flow of reactants through the catalyst bed, but flowed instead through the porous electrode backing. Flow through the backing ''jumping'' from one channel to the next is considered unlikely due to the pressure the cell was under when fitted in the testing apparatus. This pressure would compress the backing, making flow through these areas more difficult. The backing of these electrodes is ca. 350 μm thick when uncompressed. In comparison, the depth of catalyst bed, as discussed in Section 2, was 810 μm. Thus, provided the void fraction in the backing was slightly greater than that in the catalyst bed, it is reasonable that 35% of the flow could traverse through the backing. Unfortunately, the PFR in parallel with a bypass model did not accurately predict the conversion of the non-ideal reactor at lower feed rates, where the true conversion surpassed the prediction of the model. Presumably, this is because at the lower flow rates more mixing occurred between the flow in the catalyst bed and the parallel bypass flow in the electrode backing. Surprisingly, the lowered effective catalyst model, used to construct Fig. 11, fit the data from the IRFC without an MEA as well or better than any other model, so it was chosen to model the non-ideality of the IRFC reactor.

From a system design perspective the feed bypass created by the presence of the anode with a porous carbon backing as the reactor bed ''ceiling'' is troublesome, but not necessarily a fatal flaw for the IRFC. It should be remembered that the percentage of feed lost in the bypass is proportional to the thickness of the anode/backing divided by the total distance between the bottom of the catalyst bed and the membrane (i.e. the depth of the catalyst bed plus the thickness of the anode/backing). Thus, if the catalyst bed is made deeper and the anode backing made thinner, the percentage of feed lost through the bypass could be reduced. This is not an unreasonable design constraint. The depth of the catalyst bed used for this study was purposely made quite shallow to keep the total mass of catalyst, and thus, the total methanol conversion rate, low. This was done because it is beneficial, from a mathematical standpoint, to have lower conversions when fitting a model to kinetic data. However, in a practical IRFC, the mass of catalyst would likely be greater, and thus, the depth of the channel greater. Furthermore, a thick hydrophobic backing is unnecessary for a high temperature PEM because no liquid water is present, thus, the MEA could be constructed with a

much thinner gas-backing. If both of these design changes were made, it is reasonable to expect that the bypass rate could be kept below 10% of the total feed rate.

3.4. Methanol conversion in the IRFC with an MEA

To determine the effect of the MEA on the rate of methanol conversion produced by the IRFC reactor, the IRFC was assembled with an MEA, as described in Section 2, and the methanol conversion rate obtained without drawing current from the fuel cell was measured using various feed flow rates and compositions. The results from these experiments, again plotted as predicted rate of methanol conversion versus the experimentally measured conversion, are shown in Fig. 11. The black circles in this figure represent the predicted methanol conversion using the kinetic model with 0.136 g of catalyst, the true mass of catalyst in the IRFC used for these experiments. As before, the actual methanol conversion rate measured was significantly less than predicted by the model. More significantly, the actual methanol conversion rates measured in these experiments were less than the actual methanol conversion rates measured using the IRFC without an MEA (the black squares). As before, the Peppley's model was adjusted by lowering the mass of catalyst used in the calculation in order to compensate for the non-ideality of the reactor, this time to 0.065 g. The results from these calculations are plotted in Fig. 11 as the gray circles, which now lie much closer to the unity line, indicating a good correlation between the model and the experimental results. In other words, the IRFC assembled with a MEA and loaded with 0.136 g of reforming catalyst has the same rate of methanol conversion as an ideal PFR loaded with 0.065 g of catalyst, indicating that only 47.8% of actual catalyst mass was effectively utilized.

As with the previous non-ideal reactor data, several models were used to analyze the results from the IRFC with MEA. As before, the "lowered effective catalyst mass" model, used for the calculation of Fig. 11, was found to fit the data the best. The PFR in parallel with a bypass model also fit the data well at higher feed rates, where it predicted that ca. 47% of the feed flow bypassed the reactor bed completely. The conclusion drawn is that somehow the addition of the MEA increased the cross-sectional area in which the feed could pass without coming in contact with active catalyst. Since the backing thickness and void fraction are the same in this experiment as in the experiment using the IRFC without an MEA, the only possibility is that some of the catalyst has lost it's activity. Given the earlier result that ca. 65% of the flow passed through the catalyst (the remained 35% passing through the backing), and the present result that now 53% passed through the catalyst, results in the conclusion that 53/65, or ca. 81% of the catalyst bed remains active. This result compares well with the result from the "lowered effective catalyst mass" model, which predicts that 0.065/0.080, or 81% of the effective catalyst present in the IRFC remains active.

The ca. 20% loss in active catalyst is most likely a direct effect of the H_3PO_4 acid introduced by the MEA. Visual evidence of the effect of the acid was often noticeable at the end of these experiments, when disassembling the IRFC. Inspection of the reforming catalyst bed, after removing the MEA "ceiling", revealed that the upper most layer of the catalyst had turned from its normal black, to a reddish copper color. This color was never observed when the IRFC was assembled without a H_3PO_4 containing MEA. It is likely that during the assembly of the IRFC and the subsequent heating up to operating temperature (during which the catalyst bed was purged with He), a small amount of H_3PO_4 leached from the MEA and into the upper layer of the catalyst bed, dissolving the Cu and ZnO. Upon introduction of methanol and water, H_2 began to form, shifting the electrochemical potential within the anode chamber to more reductive potentials. This resulted in most of the Cu ions dissolved in the H_3PO_4 to be reduced, plating out on any surface in electrical contact with the anode and forming the reddish (and unfortunately, catalytically inactive) copper metal that was observed.

The fact that ca. 20% of the reforming catalyst was made inactive by the H_3PO_4 leaching from the MEA shows that the hydrophobic gas-backing, which was intended to keep the H_3PO_4 from reaching the reforming catalyst, did not adequately serve its intended purpose. In some sense, 20% is a relatively small amount; considering that in a practical IRFC the depth of the catalyst bed would be greater, and thus, the percentage of catalyst corrupted by H_3PO_4 would be reduced. However, it must be taken into account that a practical IRFC would likely be cycled on and off repeatedly, and during each extended off period, the acid would have an opportunity to leach further into the reforming catalyst bed, dissolving a greater amount of catalyst. The concept of limiting the leaching of H_3PO_4 by use of a hydrophobic gas-backing may be adequate if the procedure for construction of the MEAs were different. Recall from Section 2 that the electrodes (with backing attached) were soaked in a solution of ethanol and phosphoric acid, and then they were dried. If a different method was used, in which the acid was applied only on the electrode side, avoiding any acid getting into the backing, then the backing may have served its intended purpose. Alternatively, if a suitable catalyst could be found that was tolerant to a limited amount of H_3PO_4, this problem could be avoided entirely. However, until this is solved, the problem of H_3PO_4 leaching into the reforming catalyst bed is critical, and likely fatal to any IRFC designed to be cycled on and off.

3.4.1. Methanol conversion in the IRFC with an MEA while drawing current

The final experiments using the IRFC were designed to study the effect of extracting H_2 from the reforming catalyst bed by drawing current from the fuel cell. The results from these experiments appear in Fig. 12, and are plotted as methanol conversion versus electrical current. The solid line

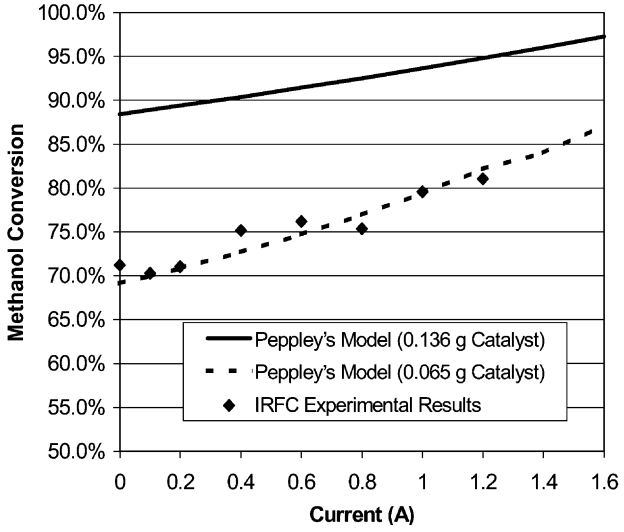

Fig. 12. Methanol conversion vs. applied current: as measured from the IRFC (black diamonds); as predicted by the Peppley's model-based using the true catalyst mass of 0.136 g (solid line); and as predicted by the kinetic model using a reduced catalyst mass of 0.065 g to take into account non-ideality (hyphenated line).

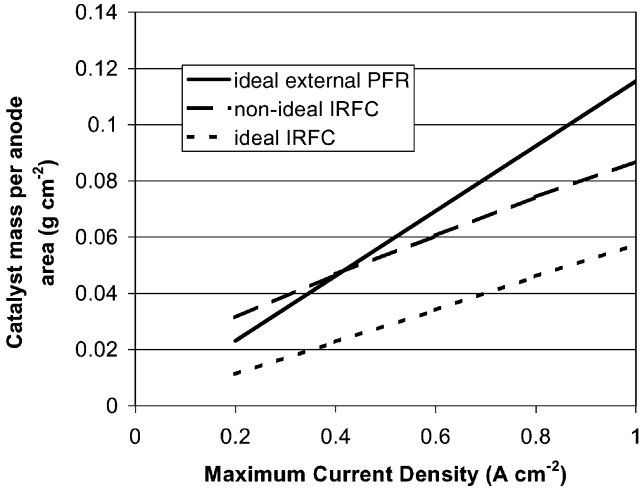

Fig. 13. The projected catalyst mass per anode area required for 95% conversion of methanol vs. the designed maximum current density of the fuel cell for an ideal external PFR (solid line), an non-ideal IRFC (dashed line), and for an ideal IRFC (hyphenated line). Calculations used Peppley's model, assumed 90% H_2 utilization, constant H_2 extraction rate along length of the IRFC, temperature of 225 °C, and a water/methanol feed ratio of 2. Geometry of the IRFC was calculated assuming reactor bed occupies 50% of anode surface area.

in this figure represents the theoretically calculated methanol conversion using the kinetic model with the full 0.136 g of catalyst (the ideal case). The hyphenated line is the methanol conversion predicted by the power law model with the reduced 0.065 g of catalyst to take into account the non-ideality of the IRFC reactor. The predicted conversion as a function of current was calculated by assuming that the H_2 extraction due to drawing electrical current was constant as a function of catalyst mass (or reactor length). Thus, the molar flow rate of H_2 at any point in the reactor bed could be expressed as

$$F_{\mathrm{H}} = F_{\mathrm{H0}} + 3F_{\mathrm{M0}}X - \frac{I}{2F}\frac{m}{m_{\mathrm{T}}} \tag{16}$$

where F_{H} is the molar flow of H_2 at any conversion, X, F_{H0} and F_{M0} are the molar feed rate of H_2 and methanol, respectively, I the total current, F the Faraday's constant, m the mass of catalyst already passed through, and m_{T} is the total mass of catalyst in the reactor. Mathematically, Eq. (16) was used in place of the expression for H_2 flow rate given previously in Eq. (5). This approximation assumes that the current density in the anode is constant, that the reforming catalyst is distributed evenly across the anode, and that diffusion occurs only perpendicular to the direction of flow.

It is clear from Fig. 12 that the actual conversion obtained (black diamonds) correlated well with the predicted conversion, once reactor non-ideality was taken into account (hyphenated line). The positive slope to these lines is due to the enhanced kinetics obtained when the H_2 product is extracted from the reactor bed, as was discussed in Section 1.2. The slope of the solid line is not as great as the slope to the hyphenated line because the predicted methanol conversion (and hence, the rate of H_2 production) is much greater for the case represented by the solid line. Thus, the same amount of current consumes a smaller percentage of the available H_2, resulting in a diminished acceleration of the reforming reaction at greater methanol conversion rates. Of particular note in Fig. 12 is that slope of the actual data obtained from the IRFC correlates well with the slope predicted by the theory, demonstrating experimentally that extraction of H_2 due to operation of the fuel cell does accelerate the reforming reaction.

Acceleration of the reforming reaction was one of the key advantages of the IRFC discussed in Section 1. With the results obtained in this study, it is now possible to make a reasonable estimate as to how much of an advantage this may be. Fig. 13 shows the catalyst mass per anode area required for 95% (or greater) conversion of methanol as a function of the designed maximum current density of the cell, for an ideal PFR, an ideal IRFC, and a non-ideal IRFC. For these calculations, it was assumed 90% H_2 utilization in the fuel cell, constant H_2 extraction (for the IRFC only), 225 °C reactor temperature, and a water to methanol molar feed ratio of 2. Thus, Fig. 13 plots on the y-axis, the amount of catalyst that would be needed to reform the amount of methanol required to support a current density shown on the x-axis divided by (0.90×0.95). For the non-ideal IRFC, it was assumed that the effective catalyst mass was proportional to the depth of the catalyst bed, which was determined by assuming a catalyst density of 1.1 g cm^{-3} and that 50% of the anode area would be occupied by the catalyst bed (the remaining 50% being used for current collection). Note that in Fig. 13, the slope of the ideal PRF line is much greater than the slope of the ideal IRFC line. This is due to the

acceleration of the reforming reaction due to extraction of H_2 from the IRFC. However, more interesting are the relative positions of the ideal PFR line and the non-ideal IRFC line, which cross just above 400 mA cm^{-2}. As discussed previously, due to the geometry of the IRFC, flow through the IRFC becomes more ideal as the depth of the catalyst bed increases. This effect is taken into account in Fig. 13. Thus, below 400 mA cm^{-2} the geometry of the non-ideal IRFC is such that more catalyst is required than would be for an ideal external PFR. However, above 400 mA cm^{-2}, the acceleration of the reforming reaction due to H_2 extraction becomes more important that the non-ideal geometry of the IRFC, and now less catalyst would be required in the non-ideal IRFC than in an ideal external PFR.

3.5. Increased tendency for coking

Coking is a term commonly used to describe the undesirable co-production of solid carbon as a product from an organic material. Formation of solid carbon on the high surface area $CuO/ZnO/Al_2O_3$ catalyst during steam reforming can quickly reduce its effectiveness by blocking the pores within the catalyst particles. This is a particular concern in the IRFC because the reforming catalyst is integrated into the fuel cell, so it cannot easily be replaced and, therefore, it must have the same life expectancy as the MEA. In conventional methanol-steam reformation reactors the formation of coke is of little concern provided the temperature at all points within the reactor bed remains above ca. 200 °C and the molar water to methanol ratio is >1; conditions in which solid carbon formation is not favored thermodynamically. Unfortunately, by enabling the in situ extraction of H_2 from the reactor, the IRFC can shift the chemical equilibrium such that the production of solid carbon becomes thermodynamically favored.This situation is shown graphically in Fig. 14, which is a tertiary diagram of the carbon–hydrogen–oxygen system at 500 K and 1 atm (for more information on the equilibrium compositions of C–H–O systems at atmospheric pressure, see Cairns and Tevebaugh [14]) A curved line representing the boundary between regions in which solid carbon is, and is not, thermodynamically favored divides the area within the triangle of this figure. Also in Fig. 14 are four dashed lines (for four different water to methanol feed ratios), representing the changing atomic composition within the IRFC reactor bed as H_2 is removed from the reactor bed. The left most point of each dashed line is the composition within the reactor when no H_2 has been removed, and the right most point of each dashed line is the composition when all of the available H_2 has been removed (the equivalent of 100% methanol conversion with 100% hydrogen utilization). It is clear from Fig. 14 that the water to methanol feed ratio of an IRFC operating at 500 K must be greater than ca. 2 in order to avoid crossing into the region in which production of solid carbon is thermodynamically favored as the H_2 produced by the reforming reaction is consumed by the fuel cell.

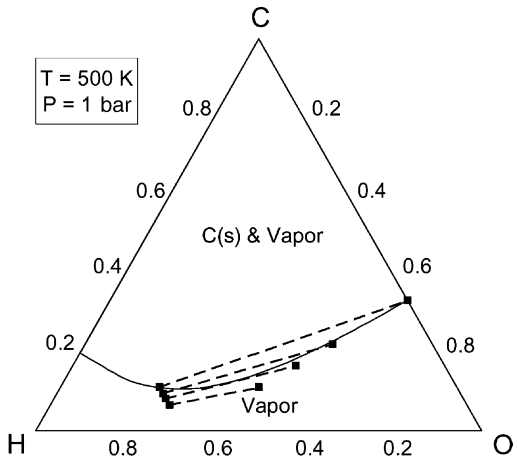

Fig. 14. Tertiary diagram of the C–H–O system: the curved line represents the border between regions, where solid carbon is thermodynamically stable (top) and where it is unstable (bottom). The four dashed lines represent the composition within the IRFC as H_2 is consumed by the fuel cell for four different water to methanol feed ratios: 1.0, 1.5, 2.0, and 3.0, as shown from uppermost to lowermost, respectively.

It is important to note that even though certain compositions of water, methanol, hydrogen and carbon dioxide may lie within the coking region, it does not insure that coking will occur. Even within this region, for solid carbon to form at appreciable rates there must be a reaction mechanism for its production that is energetically viable. Conversely, it should not be automatically assumed that coking would not occur when the chemical composition within the steam-reformation reactor is outside of the thermodynamically stable region for solid carbon. This is particularly true when the composition of the chemical system lies near a phase-change line such as is the case for the steam-reforming reaction at ca. 500 K and 1 atm. Thus, thermodynamically derived plots such as Fig. 14 act only as a caveat; the true reaction products (at least within finite time) are determined by the respective kinetics of the competing reaction mechanisms. This phenomena was demonstrated in a study conducted by Amphlett et al. [15], in which no coking was observed in a number of reactions where the conditions thermodynamically favored coking.

4. Conclusions

The kinetic expression put forth by Peppley et al. was found to be adequate for modeling the behavior of the methanol-steam reformation reaction. Using this model, predicted conversion from a PFR was compared with measured methanol conversions from an IRFC with and without a H_3PO_4 containing MEA. It was found that methanol conversion rates in the IRFC without an MEA (and without H_2 extraction) were significantly less than for an ideal PFR with an equal amount of catalyst. This is likely due to the non-ideal flow through (or around) the catalyst bed. This non-ideality could be taken into account in the model by

reducing the effective catalyst mass to 59% of the actual mass. For the IRFC with an MEA (also without H_2 extraction), it was found that methanol conversion was reduced further. This is probably due to a portion of the catalyst being deactivated by H_3PO_4. This effect could also be model by reducing the effective catalyst mass to 48% of the actual catalyst mass. Despite the non-ideal flow caused by the design compromises inherent in an IRFC and the resulting drop in effective catalyst mass, it was projected that for fuel cell systems with a current density greater than 400 mA cm^{-2}, the IRFC would require less catalyst mass than a traditional system with external reformer. This trend is the result of an experimentally verified accelerated methanol conversion rate in the IRFC caused by the extraction of H_2 from the reforming reactor bed. Furthermore, there is reason to believe that reducing the thickness of the anode gas-backing and better containing the H_3PO_4 in the MEA could significantly improve the flow behavior within the IRFC. This would result in the catalyst mass advantage of the IRFC extending below the 400 mA cm^{-2} stated earlier. Long-term stability of the IRFC, however, needs to be investigated further.

Acknowledgements

Portions of this work were supported by DARPA under subcontract #332795 from Batelle.

References

[1] H.-F. Oetjen, V.M. Schmidt, U. Stimming, F. Trila, J. Electrochem. Soc. 142 (1996) 3838–3842.
[2] M. Inbody, R. Borup, J. Tafoya, J. Hedstrom, B. Morton, in: Proceedings of the Annual National Laboratory R&D Meeting of the DOE Fuel Cells for Transportation Program, 7–8 June 2000.
[3] J.S. Wainright, J.-T. Wang, D. Weng, R.F. Savinell, M. Litt, J. Electrochem. Soc. 142 (1995) L121.
[4] V. Pour, J. Barton, A. Benda, Coll. Czech. Chem. Commun. 40 (1975) 2923.
[5] C.J. Jiang, D.L. Trimm, M.S. Wainwright, N.W. Cant, Appl. Catal. A 97 (1993) 245–255.
[6] R.F. Mann, J.C. Amphlett, B.A. Peppley, New Energy Systems and Conversions, Universal Academy Press, Inc., 1993, pp. 613–618.
[7] C.J. Jiang, D.L. Trimm, M.S. Wainwright, N.W. Cant, Appl. Catal. A 97 (1993) 145–158.
[8] B.A. Peppley, J.C. Amphlett, L.M. Kearns, R.F. Mann, Appl. Catal. A 179 (1999) 21–29.
[9] B.A. Peppley, J.C. Amphlett, L.M. Kearns, R.F. Mann, Appl. Catal. A 179 (1999) 31–49.
[10] V. Jalen, J. Giner, Investigation relating to methanol–air fuel cells: thermally integrated in situ reformer, an internal report of work commissioned by the US Army, 1984.
[11] S.R. Samms, R.F. Savinell, J. Electrochem. Soc., 2003 (submitted for publication).
[12] R.F. Savinell, M.H. Litt, US Patent 5,716,727 (1998).
[13] F.P. Incropera, D.P. DeWitt, Fundamentals of Heat and Mass Transfer, 4th Edition, Wiley, New York, 1996.
[14] E.J. Cairns, A.D. Tevebaugh, J. Chem. Eng. Data 9 (1964) 453–462.
[15] J.C. Amphlett, M.J. Evans, R.A. Jones, R.F. Mann, R.D. Weir, Can. J. Chem. Eng. 59 (1981) 720–727.